Seasonal variation of nitryl chloride and its relation to gas-phase precursors during the JULIAC campaign in Germany

Zhaofeng Tan[1], Hendrik Fuchs[1,4], Andreas Hofzumahaus[1], William J. Bloss[3], Birger Bohn[1], Changmin Cho[1], Thorsten Hohaus[1], Frank Holland[1], Chandrakiran Lakshmisha[1], Lu Liu[1], Paul S. Monks[2], Anna Novelli[1], Doreen Niether[1], Franz Rohrer[1], Ralf Tillmann[1], Thalassa Valkenburg[2], Vaishali Vardhan[1,a], Astrid Kiendler-Scharr[1,4], Andreas Wahner[1], Roberto Sommariva[2,3]

[1] Institute of Energy and Climate Research, IEK-8: Troposphere, Forschungszentrum Jülich GmbH, Jülich, Germany

[2] School of Chemistry, University of Leicester, Leicester, UK

[3] School of Geography, Earth and Environmental Sciences, University of Birmingham, Birmingham, UK

[4] Physikalisches Institut, Universität zu Köln, Köln, Germany

[a] now at, Department of Chemistry, University College Cork, Ireland

Correspondence: Zhaofeng Tan (zh.tan@fz-juelich.de) and Roberto Sommariva (rs445@le.ac.uk)

Abstract. Ambient measurements of nitryl chloride ($ClNO_2$) were performed at a rural site in Germany covering 3 periods in winter, summer, and autumn 2019 as part of the JULIAC campaign (Jülich Atmospheric Chemistry Project) that aimed for understanding the photochemical processes in air masses typical for mid-west Europe. Measurements were conducted at 50 m above ground, which was ~~most~~mainly located ~~mainly at~~in the nocturnal boundary layer and thus uncoupled from local surface emissions. $ClNO_2$ is produced at nighttime by heterogeneous reaction of dinitrogen pentoxide (N_2O_5) on chloride ~~ion~~ (Cl^-) containing aerosol. Its photolysis ~~at~~during the day is of general interest as it produces chlorine (Cl) atoms that react with different atmospheric trace gases forming radicals. The highest observed $ClNO_2$ mixing ratio was 1.6 ppbv (15-min average) ~~in~~ during the ~~middle of one~~ night ~~in~~of September 20. Air masses reaching the measurement site either originated from long-range transport from the southwest and had an oceanic influence or circulated in the nearby region and were influenced by anthropogenic activities. Nocturnal maximum $ClNO_2$ mixing ratios were around 0.2 ppbv if originating from long-range transport in nearly all seasons, while values were higher ranging from 0.4 to 0.6 ppbv for regionally influenced air. The chemical composition of long-range transported air was similar in all

29 investigated seasons, while the regional air exhibited larger differences between the seasons. The N_2O_5

30 necessary for $ClNO_2$ formation comes from the reaction of nitrate radicals (NO_3) with nitrogen dioxide

31 (NO_2), where NO_3 itself is formed by reaction of NO_2 with ozone (O_3). Measured concentrations of

32 $ClNO_2$, NO_2 and O_3 were used to quantify $ClNO_2$ production efficiencies, i.e., the yield of $ClNO_2$

33 formation per NO_3 radical formed, and a box model was used to examine the idealized dependence of

34 $ClNO_2$ on the observed nocturnal O_3 and NO_2 concentrations. Results indicate that $ClNO_2$ production

35 efficiency was most sensitive to the availability of NO_2 rather than that of O_3 and increase with decreasing

36 temperature. The average $ClNO_2$ production efficiency was highest in February and September with

37 values of 18% and was lowest in December with values of 3%. The average $ClNO_2$ production

38 efficiencies were in the range of 3 and 6 % from August to November for air masses originating from

39 long-range transportation. These numbers are at the high end of values reported in literature indicating the

40 importance of $ClNO_2$ chemistry in rural environments in mid-west Europe.

41 # 1 Introduction

42 Nitryl chloride ($ClNO_2$) is an important nocturnal reservoir for nitrogen oxides (Brown and Stutz, 2012),

43 because it accumulates during the night and photolyzes to nitrogen dioxide (NO_2) and a chlorine atom

44 (Cl) after sunrise in the morning (Reaction R1).

45 $ClNO_2 + hv \rightarrow NO_2 + Cl$ (R1)

46 Chlorine atoms are a highly reactive oxidant in the atmosphere, initiating, for example, the degradation of

47 volatile organic compounds (VOCs) and thereby contributing to the formation of ozone (O_3) and other

48 pollutants (Simpson et al., 2015;Thornton et al., 2010;Mielke et al., 2011;Young et al., 2012). In some

49 studies, $ClNO_2$ was shown to increase the daily ozone production from sub ppbv levels to mixing ratios of

50 up to 10 ppbv, so that $ClNO_2$ chemistry contributed substantially to photochemical ozone production

51 (Osthoff et al., 2008;Wang et al., 2016;Sommariva et al., 2021).

52 $ClNO_2$ formation is initiated by the heterogeneous reaction of dinitrogen pentoxide (N_2O_5) on aqueous

53 surfaces that contains chloride (Cl^-) ~~ions~~ (Roberts et al., 2009;George and Abbatt, 2010;Osthoff et al.,

54 2008;Thornton et al., 2010). The entire chemical reaction chain is described as McDuffie et al. (2018a):

55 $NO_2 + O_3 \rightarrow NO_3 + O_2$ (R2)

56 $NO_3 + NO_2 \rightarrow N_2O_5$ (R3a)

57 $N_2O_5 \rightarrow NO_3 + NO_2$ (R3b)

58 $$N_2O_{5\,(g)} + aerosol_{(aq,Cl^-)} \rightarrow \varphi \times \left(ClNO_{2\,(g)} + HNO_{3\,(aq)}\right) + (1-\varphi) \times 2\,HNO_{3\,(aq)} \tag{R4}$$
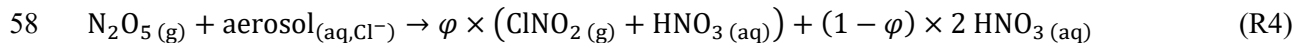
59 where φ is the yield ($\cancel{0<}\,0 \leq \varphi\,\cancel{<1}\leq 1$) of gaseous $ClNO_2$ when N_2O_5 is taken up by aerosol.

60 $$NO_3 + VOCs \rightarrow prod. \tag{R5}$$

61 At night, nitrate radicals (NO_3) are produced by reaction of NO_2 with O_3 (Reaction R2), which then react

62 with another NO_2 to form N_2O_5 (Reaction R3a). N_2O_5 decomposes thermally back to NO_2 and NO_3

63 (Reaction R3b). The forward and back reactions constitute a fast thermal equilibrium between NO_3 and

64 N_2O_5 that is established ~~within a minute at room temperature. Uptake of N_2O_5 on aqueous aerosol~~

65 ~~produces $ClNO_2$, when the particulate phase of the aerosol contains dissolved chloride ions.~~ quickly

66 established at temperatures typically found in the lower troposphere (Brown and Stutz, 2012). Uptake of

67 N_2O_5 on aqueous aerosol produces $ClNO_2$, when the particulate phase of the aerosol contains dissolved

68 chloride. The yield (φ) of $ClNO_2$ is a complex function of various parameters such as temperature, aerosol

69 water content, and chemical composition of the aerosol that influence both uptake of N_2O_5 into the

70 particles (McDuffie et al., 2018a) and the subsequent aqueous phase chemistry leading to the formation of

71 $ClNO_2$ (McDuffie et al., ~~2018b~~2018a). The uptake of N_2O_5 (Reaction R4) and the reaction of NO_3 with

72 VOCs (Reaction R5) constitute an overall loss term for the sum of NO_3 and N_2O_5, because the fast

73 equilibrium between NO_3 and N_2O_5. HNO_3 formation by Reaction R4 is an important atmospheric sink

74 for atmospheric nitrogen oxides in the lower atmosphere, because HNO_3 photolysis is slow so that most

75 of the produced HNO_3 does not reform NO_2, but is removed from the atmosphere by deposition (Brown

76 and Stutz, 2012). During the daytime, NO_3 is destroyed by photolysis or by reaction with nitric oxide

77 (NO). The thermal equilibrium between NO_3 and N_2O_5 thus leads to a rapid depletion of N_2O_5 at day.

78 Therefore, significant concentrations of N_2O_5~~,~~ (the precursor of $ClNO_2$~~,~~) are usually only present at night.

79 Previous studies reporting $ClNO_2$ measurements in North America (Osthoff et al., 2008;Thornton et al.,

80 2010;Mielke et al., 2011;Wagner et al., 2012;Young et al., 2012;Mielke et al., 2013;Riedel et al.,

81 2013;McDuffie et al., 2018b;McNamara et al., 2020), Asia (Tham et al., 2016;Wang et al., 2016;Liu et

82 al., 2017;Wang et al., 2017a;Wang et al., 2017b;Le Breton et al., 2018;Yun et al., 2018;Zhou et al.,

83 2018;Yan et al., 2019;Jeong et al., 2019;Lou et al., 2022) and Europe (Phillips et al., 2012;Bannan et al.,

84 2015;Priestley et al., 2018;Sommariva et al., 2018) have shown that $ClNO_2$ is present in various

85 environments even at a distance from the coast, indicating that other sources of chloride than sea spray

86 contribute to the availability of chlorine for the formation of $ClNO_2$. Observed mixing ratios of $ClNO_2$ in

87 the atmosphere range from a few hundred pptv to several ppbv exhibiting significant spatial and temporal

88 variations.

89 Despite the large variation in $ClNO_2$ concentrations and its potentially important contribution to

90 photochemistry, systematic investigations of seasonal differences of $ClNO_2$ concentrations are sparse,

91 because $ClNO_2$ is not regularly measured at monitoring stations, but during intensive field campaigns,

92 which last typically only a few weeks. Sommariva et al. (2018) reported $ClNO_2$ measurements at three

93 different locations in the United Kingdom in all four seasons showing a clear seasonal variation with

94 maximum concentrations in spring and winter. Another study by Mielke et al. (2016) reporting the

95 seasonal behavior of $ClNO_2$ in Calgary, Canada, also showed maximum mixing ratios of $ClNO_2$ of up to

96 330 pptv in winter and spring. ~~Given the ubiquitous nature of $ClNO_2$ and its importance to enhance~~

97 ~~atmospheric oxidation processes, more studies are needed to broaden the knowledge about atmospheric~~

98 ~~$ClNO_2$ concentrations, its seasonal behavior and its distributions in environments with different chemical~~

99 ~~conditions.~~

100 The large variability of $ClNO_2$ concentrations in the atmosphere is due to the complexity of its formation

101 mechanism (Reactions R2 – R5) and the variability of its precursor concentrations. Assuming steady state

102 for the sum of NO_3 and N_2O_5 concentrations, the following relationship holds

103 $$\frac{d[NO_3+N_2O_5]}{dt} \cong 0 = k_2[NO_2][O_3] - k_{NO_3}[NO_3] - k_4[N_2O_5]$$ (Eq. 1)

104 where k_{NO_3} represents the pseudo first-order rate constant for NO_3 loss mainly dominated by reactions

105 with atmospheric VOCs (Reaction R5) at night with no fresh NO emissions. Considering the thermal

106 equilibrium between NO_3 and N_2O_5, the $[NO_3]$ can be replaced by $[N_2O_5]/(K_{eq}(T)[NO_2])$ where $K_{eq}(T)$

107 is temperature dependent and equals to the ratio of the reaction rate constants of the thermal equilibrium,

108 i.e. k_{3a} to k_{3b} (Reaction R3a and b). Equation 1 can be solved for

109 $$[N_2O_5] = \frac{K_{eq}(T)[NO_2]}{k_{NO3} + K_{eq}(T)[NO_2]k_4} \cdot k_2[NO_2][O_3]$$ (Eq. 2)

110 The production rate of $ClNO_2$ is then

111 $$P_{ClNO2} = \varphi \cdot k_4 \cdot [N_2O_5] = \varphi \cdot \left(\frac{K_{eq}(T)[NO_2]k_4}{k_{NO_3} + K_{eq}(T)[NO_2]k_4}\right) \cdot k_2[NO_2][O_3]$$ (Eq. 3)

112 A production efficiency ε for $ClNO_2$ can be defined from this relationship

113 $$\epsilon_{ClNO2} = \frac{P_{ClNO2}}{k_2[NO_2][O_3]} = \varphi \left(\frac{K_{eq}(T)[NO_2]k_4}{k_{NO3} + K_{eq}(T)[NO_2]k_4}\right)$$ (Eq. 4)

114 It represents the formation rate of $ClNO_2$ from aerosol per NO_3 produced by the reaction of NO_2 with O_3

115 in the gas phase. Equations Eq. 3 and Eq. 4 describe the expected influences on the $ClNO_2$ formation by

116   its precursors NO_2 and O_3, by temperature and NO_2 controlling the equilibrium between NO_3 and N_2O_5,

117   and the competing loss reactions of NO_3 and N_2O_5 via Reactions R5 and R4, respectively. φ is an

118   additional variable depending on the properties of the aerosol and specifically on its chloride content, as

119   mentioned above.

120   This study presents $ClNO_2$ measurements performed during the Jülich Atmospheric Chemistry Project

121   (JULIAC) campaign in three seasons (i.e. winter, summer, and autumn 2019). The JULIAC campaign

122   aimed to investigate the seasonal and diurnal variations of the atmospheric oxidation capacity at a rural

123   site that is typical for mid-west Europe. To minimize the impact of emissions from local sources, the air

124   was drawn from 50 m above ground ensuring that air is sampled from above the surface layer during

125   nighttime and flowed through the large environmental chamber SAPHIR at Forschungszentrum Jülich,

126   Germany. In this work, the seasonal variation of $ClNO_2$ concentrations and its formation are investigated.

127   ~~Empirical~~As mentioned above, previous studies have demonstrated that $ClNO_2$ concentrations show

128   significant seasonal variations (Mielke et al., 2016;Sommariva et al., 2018). However, intensive seasonal

129   measurements in central Europe, to our knowledge, have not been performed so far. Given the ubiquitous

130   nature of $ClNO_2$ and its importance to enhance atmospheric oxidation processes, more detailed studies are

131   needed to broaden our knowledge of atmospheric $ClNO_2$ levels, its seasonal behavior and its distribution

132   in environments with different chemical conditions. In addition, this work presents empirical production

133   efficiencies of $ClNO_2$ ~~are~~ determined from the nighttime measurements of $ClNO_2$, NO_2 and O_3 and

134   analyzed for their seasonal variations and origin of air masses, ~~which is~~ a prerequisite to

135   ~~determine~~understand the contribution of $ClNO_2$ to radical photochemistry ~~for~~under the chemical and

136   meteorological conditions encountered in this campaign. ~~A~~Finally, a chemical box model ~~helps~~is used

137   here to understand the dependence of $ClNO_2$ formation and production efficiency on the observed

138   nocturnal O_3 and NO_2 concentrations. The measurements and analysis presented in this paper help to

139   illustrate the seasonal variability of $ClNO_2$ concentrations and shed light on the factors that control its

140   production in different seasons.

141   ## 2 Methods

142   **2.1 The JULIAC campaign**

143   The JULIAC campaign was conducted in 2019 in the atmospheric simulation chamber SAPHIR on the

144   campus of Forschungszentrum Jülich, which is located at a rural site in Germany (50.91° N, 6.40° E).

145   The SAPHIR chamber consists of a double-wall Teflon film (volume: (277 ± 3) m^3) (Bohn et al.,

146   2005;Rohrer et al., 2005). Its high volume to surface ratio (1 m^2/m^3) minimizes air-surface interactions

147 within the chamber. The time scale of mixing is about 1 minute ensured by two fans that are operated

148 inside the chamber.

149 During this study, ambient air was drawn from 50 m height above ground into the chamber (Fig. S1,

150 Supporting Information). At this height, the air is expected to be decoupled from the surface layer during

151 the night, so that the air composition is not directly impacted by sources at the ground or deposition of

152 trace gases to the Earth's surface (Section 3.3). The inlet line (SilcoNert® coated stainless steel, inner

153 diameter: 104 mm) was mounted at a tower (JULIAC tower) next to the chamber. A fast flow rate of 660

154 m^3/h resulted in a residence time of the air inside the inlet line of approximately 4 s. The short residence

155 time and the inertness of the Silconert coating of the inlet line minimized loss and chemical changes of

156 the air before entering the SAPHIR chamber. The potential loss of trace gases in the inlet line was tested

157 for O_3, NO, NO_2, and CO and was found to be less than 5%.

158 Instruments could either sample air directly from the inlet line or the chamber volume. In the latter case,

159 part of the total air drawn through the inlet at the JULIAC tower flowed through the SAPHIR chamber

160 with a flow rate of 250 m^3/h that was controlled by a three-way valve right upstream of the injection point

161 into the chamber. The remaining part was vented. The residence time of sampled ambient air inside the

162 SAPHIR chamber was 1.1 hours calculated from the measured flow rate and the chamber volume.

163 Sampling air from the large volume of the SAPHIR chamber has the advantage that short-term variations

164 of trace gas concentrations flowed into the chamber for example due to local emissions or fast changes of

165 air masses are smoothed.

166 The JULIAC campaign consisted of four intensive measurement periods in winter (14 January to 10

167 February 2019), spring (08 April to 05 May 2019), summer (05 August to 01 September 2019), and

168 autumn (28 October to 24 November 2019). During these parts of the campaign, a large set of instruments

169 sampled air from the chamber. In addition, between each intensive measurement period, a limited set of

170 instruments for the detection of $ClNO_2$, O_3, NO, NO_2, OH reactivity, and VOCs continued measuring

171 directly from the inlet line at the JULIAC tower (Fig. S1, Supporting Information).

2.2 Instrumentation

173 A large set of instruments was deployed during the JULIAC campaign. In this work, the focus is on

174 measurements that are relevant to study the chemistry of $ClNO_2$.

175 $ClNO_2$ was measured by a chemical ionization mass spectrometry (CIMS) instrument from Leicester

176 University (THS Instruments LLC, GA, USA) operated in negative ion mode using iodide (I^-) as reagent

177   ion. $ClNO_2$ was detected at the mass to charge ratios (m/z) of 208 and 210 amu, corresponding to the two

178   isotopes of the $[I \cdot ClNO_2]^-$ ion clusters as described in Sommariva et al. (2018).

179   The CIMS instrument was calibrated by standard additions of $ClNO_2$ generated by flowing humidified air

180   containing Cl_2 (from a cylinder containing a mixture of 5 ppmv (±5%) Cl_2 in N_2, Linde AG) over a salt

181   bath containing a 1:1 mixture of NaCl and $NaNO_2$ (Sommariva et al., 2018). The resulting $ClNO_2$

182   concentration in the air was determined by measuring the NO_2 concentration after thermally decomposing

183    $ClNO_2$ to Cl and NO_2 in a glass tube heated to a temperature of 400 ℃. The NO_2 concentrations were

184   measured using a commercial NO_2 analyzer that makes use of the cavity attenuated phase-shift method

185   (CAPS, T500U, Teledyne API). The accuracy of NO_2 measurements by this analyzer is ±5%. ~~The~~

186   ~~uncertainties in the mixture of Cl_2 (±5%) and of the flow rates measured by mass flow controllers used to~~

187   ~~mix the air in the calibration system (±5%) add to the total uncertainty of the calculated $ClNO_2$~~

188   ~~concentration provided during the calibration procedure.~~ The overall accuracy of the $ClNO_2$ calibration is

189   ±17~~%. The~~%; the precision of $ClNO_2$ measurements is 13% with a 2-σ detection limit of 5.6 pptv at a 1-

190   minute time resolution.

191   The CIMS detection sensitivity depends on humidity because iodide ions form clusters with water

192    $(I \cdot (H_2O)^-)$. The water-iodine cluster is a more efficient reagent ion for producing $I \cdot (ClNO_2)^-$ clusters than

193   the I^- ion (Kercher et al., 2009). The dependence of the sensitivity on humidity was characterized with

194   calibration experiments by varying the mixing ratios of water vapor. These experiments show that the

195   sensitivity of the instrument for the detection of $ClNO_2$ decreases by 19% per 1% water vapor mixing

196   ratio (Fig. S2, Supporting Information), when the signal is normalized to the $I \cdot (H_2O)^-$ cluster signal (m/z

197   = 145). Calibrations of the instrument were performed during each measurement period using comparable

198   average humidity to that of the ambient air. The variability of the sensitivity due to the changes in

199   humidity in each 4-week long measurement period was less than ±5%. This is within the range of

200   reproducibility of calibration measurements. Therefore, the sensitivity was not corrected for the humidity

201   effect for individual data points, but an average sensitivity value was applied to all data from the entire

202   measurement period. The uncertainty due to the humidity dependence of the sensitivity and the

203   reproducibility of the calibration adds to the overall accuracy of $ClNO_2$ measurements increasing the

204   value to ±27%.

205   Photolysis frequencies inside the SAPHIR chamber were calculated from the actinic flux measured

206   outside the chamber and corrected for the reduction of radiation by shading effects and the transmission

207   of the Teflon film (Bohn et al., 2005). Ozone was detected by a UV photometer (model O342M, Ansyco).

208   Nitric oxide (NO) was measured by a chemiluminescence instrument (780TR, Eco Physics) that was also

209   used to detect NO_2 by conversion of NO_2 to NO in a blue-light photolytic converter upstream of the NO

210   analyzer. For the period after 01 December 2019, NO_2 was measured by an instrument using the iterative

211   cavity enhanced differential optical absorption spectroscopy method (ICAD1005, AirYX). The NO_2

212   measurements from the two instruments agreed well within 5%, when both instruments measured

213   concurrently. Water vapor and carbon monoxide (CO) concentrations were measured by a cavity ring-

214   down instrument (G2401, Picarro). NO_3 and N_2O_5 were measured by a custom-built cavity ring-down

215   instrument that is similar to the one described in Wagner et al. (2011).

216   Particle number concentration (for particles with a diameter > 5 nm) and size distribution (for particles

217   with a diameter between 10 and 1000 nm) were measured by a condensation particle counter (model

218   3787, TSI) and a scanning mobility particle sizer (model 3080, TSI), respectively. The aerosol surface

219   area (S_a) was calculated based on the particle number and geometric diameter in each size bin. The

220   chemical composition of particles was analyzed by an aerosol mass spectrometer (HR-TOF-AMS,

221   Aerodyne).

222   Temperature and pressure of the ambient air were measured inside the chamber and also outside the

223   chamber at different heights (2 m, 20 m, 30 m, 50 m, 80 m, 120 m) by sensors mounted at a

224   meteorological tower located approximately 200 m away from the SAPHIR chamber.

225   ## 2.3 Comparability of measurements from the chamber and the inlet line

226   Air was sampled from 50 m above the ground from the top of the JULIAC tower at all times of the

227   campaign (Fig. S1, Supporting Information). However, $ClNO_2$ concentrations were determined in the air

228   from either one of the two sampling points during the different periods of the campaign.

229   During the intensive measurement periods (i.e. in February, August, and November), air was directly

230   sampled from the SAPHIR chamber. During other times, air was sampled from the inlet system of the

231   chamber at the JULIAC tower. In both cases, measured concentrations are representative for the air from

232   50 m height. In the case of sampling from the chamber, concentrations are averaged due to the 1-hour

233   residence time of air in the chamber.

234   To make data derived from both sampling points comparable, $ClNO_2$ concentrations measured inside the

235   chamber ($C_{chamber}$) were converted to equivalent concentrations at the tip of the JULIAC inlet system

236   (C_{50m}). This can be achieved from the differential equation of concentrations taking into account dilution

237   with the flow rate (k_{flow}) and loss ($L_{chamber}$) and production ($P_{chamber}$) inside the chamber:

238     $$\frac{dC_{chamber}}{dt} = k_{flow}(C_{50m} - C_{chamber}) + P_{chamber} - L_{chamber} \qquad \text{(Eq. 5)}$$

239 The concentration in the incoming air can be iteratively determined from the time series of measured

240 concentrations inside the chamber, if loss and production processes can be quantified. The other species

241 used in this work (e.g. O3, NOx, etc.) were measured both at the tip of the JULIAC inlet and inside

242 SAPHIR. Unless otherwise specified, the measurements presented in this work were taken at the tip of the

243 JULIAC inlet, or corrected using Eq 5.

244 Production of $ClNO_2$ from the heterogeneous reaction of N_2O_5 on particles is expected to be negligible on

245 the time scale of the residence time of air in the chamber for conditions of the JULIAC campaign.

246 Chamber wall interaction could be relevant because the surface area of the Teflon film is 10^6 $\mu m^2/cm^3$,

247 i.e. several orders of magnitude larger than the surface area of ambient aerosol experienced in this

248 campaign, which were on the order of tens to hundreds of $\mu m^2/cm^3$. To quantify potential chamber

249 related loss and production processes, chamber characterization experiments were conducted (Section

250 3.1). They were analyzed by using a chemical box model, in which loss and production rates were

251 adjusted to reproduce measured $ClNO_2$ concentrations during these experiments. Temperature, relative

252 humidity, pressure, photolysis frequencies, and dilution rates determined from the air replenishment flow

253 rate were constrained to measurements in the model. The conversion of N_2O_5 to $ClNO_2$ via surface

254 reactions (Reaction R6) and the loss reactions of $ClNO_2$ on the chamber wall (Reaction R7) were included

255 in the model assuming pseudo-first order processes:

256 $N_2O_5 + wall \rightarrow ClNO_2$ (R6)

257 $ClNO_2 + wall \rightarrow products$ (R7)

258 In addition, the chemical loss of $ClNO_2$ via photolysis (Reaction R1) was considered. The results of these

259 experiments and the model analysis are discussed in Section 3.1.

3 Results and Discussion

3.1 Chamber effects on measured $ClNO_2$ concentrations

262 Two types of experiments were performed to characterize the chamber properties with respect to wall

263 interaction of NO_3, N_2O_5, and $ClNO_2$. In these chamber characterization experiments, only a small

264 replenishment flow of pure synthetic air compensated for leakages and extraction of air by instruments.

265 This led to a low dilution of trace gases with a rate that is equivalent to a lifetime of 17 hours in contrast

266 to the 1-hour lifetime during the operation of the chamber in the JULIAC campaign.

267   Three experiments were conducted (05, 06, and 07 February 2019) to test whether $ClNO_2$ was exclusively
268   lost by photolysis in the chamber or whether other processes, such as wall loss, contributed to the $ClNO_2$
269   removal. These experiments started with flowing ambient air through the SAPHIR chamber during the
270   night like in the operational mode of the JULIAC campaign (Section 2.1). The high flow was stopped
271   before sunrise (around 06:00 UTC) and the small replenishment flow was started. The evolution of trace
272   gas concentrations was observed until around 12:00 UTC while the air was exposed to sunlight. The N_2O_5
273   concentration decreased rapidly to zero after sunrise and thus no further $ClNO_2$ could be produced from
274   N_2O_5 conversion and $ClNO_2$ concentrations also decayed during the morning.

275   Measured concentrations are compared to calculation using a chemical box model (Section 2.3)
276   considering losses of $ClNO_2$ by dilution, photolysis, and potential wall loss. Whereas loss rates for
277   dilution and photolysis are constrained to measurements, the wall loss rate constant is adjusted to match
278   observed $ClNO_2$ concentrations. This results in a wall loss rate constant for $ClNO_2$ of 2.1×10^{-5} s^{-1}. This
279   value is on the same order of magnitude as the loss rate constant of $ClNO_2$ due to photolysis (4.1×10^{-5} s^{-1}
280   at noon) and dilution (1.5×10^{-5} s^{-1}) for the experimental conditions of the characterization experiments.
281   Due to the higher chamber flow rate used during the JULIAC campaign, the dilution rate is an order of
282   magnitude higher (2.5×10^{-4} s^{-1}) than during the characterization experiments. Therefore, the wall loss rate
283   is only 8% of the dilution rate, and can be neglected in the further data analysis.

284   Additional three experiments were performed to characterize potential $ClNO_2$ formation from
285   heterogeneous reactions of N_2O_5 on the chamber wall. In these experiments (18 September, 18 October,
286   and 19 November 2019), NO_2 and O_3 were added into the dark chamber filled with pure, dry, or
287   humidified synthetic air. These experiments lasted for about 10 hours to observe the decay of NO_2 and O_3
288   concentrations and the accumulation of $ClNO_2$.

289   Fig.Figure 1 shows measured concentrations for the experiments performed on 19 November. In this
290   experiment, the chamber air was humidified (RH=60%) and 28 ppbv of NO_2 and 80 ppbv of O_3 were
291   injected to produce NO_3 and N_2O_5. NO_3 mixing ratios were below the limit of detection (about a few
292   pptv) of the cavity ring-down instrument.

293   N_2O_5 measurements reached maximum mixing ratios of 0.17 ppbv shortly after the O_3 injection and
294   decreased afterward (Fig. 1). Also, $ClNO_2$ production was observed shortly after the ozone addition, when
295   N_2O_5 was present. Because the air was particle-free, one possible explanation for the formation of $ClNO_2$
296   is heterogeneous reaction of N_2O_5 on the chamber wall that may contain chloride, which could have been
297   deposited, for example, during previous experiments with ambient air.
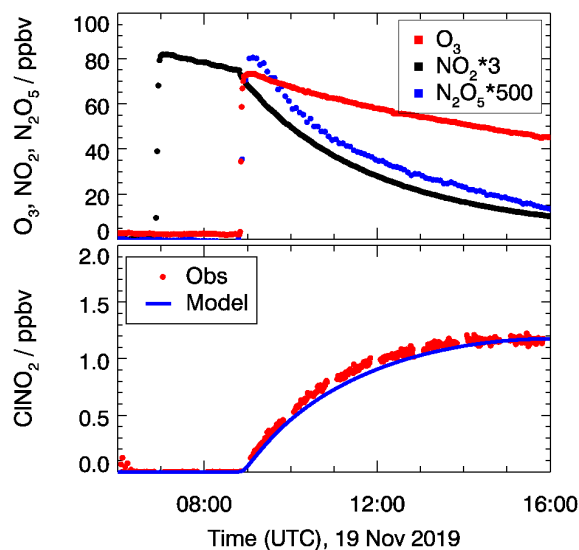
Figure 1. Chamber experiment to characterize $ClNO_2$ production from N_2O_5 conversion on the chamber wall in the dark on 19 November 2019. $ClNO_2$ concentrations are compared to model calculations taking conversion from N_2O_5 to $ClNO_2$ (Reaction R6) into account. A reaction rate constant of 8.2×10^{-6} s^{-1} is required to reproduce measured $ClNO_2$ concentrations.

The values of the conversion rates from N_2O_5 to $ClNO_2$ (Reaction R6) that are required to match the measured $ClNO_2$ concentrations in the model calculations are $k_{R6} = 4.0 \times 10^{-6}$ s^{-1}, 2.0×10^{-6} s^{-1}, and 8.2×10^{-6} s^{-1} for the experiments on 18 September, 18 October and 19 November 2019, respectively.

During the JULIAC campaign, however, the potential contribution of $ClNO_2$ formation from N_2O_5 conversion on the chamber film was negligible. Taking the typical nocturnal N_2O_5 mixing ratio of about 50 pptv, the expected $ClNO_2$ production rate from N_2O_5 conversion on the chamber wall was about 1.5 pptv/h using the upper limit value of k_6 derived from the characterization experiments. This is less than 1% of the ambient $ClNO_2$ mixing ratio of up to several hundred pptv in the ambient air that is flowed into the chamber. Therefore, no corrections are needed for the interpretation of $ClNO_2$ measurements in the chamber.

Overall, the results of the characterization experiments allow to simplify the back-calculation of the $ClNO_2$ concentrations in the sampled air from measured concentrations in the chamber (Eq. 5). The chemical production rates and the deposition rates for $ClNO_2$ and N_2O_5 on the chamber walls can be neglected and only photolysis needs to be considered as a destruction process for $ClNO_2$ during the daytime. For nighttime conditions, $ClNO_2$ concentrations in the incoming air can be determined solely from the flow rate and the measured $ClNO_2$ concentration inside the chamber.

3.2 Overview of measurements

In order to determine the origin of air masses sampled at the measurement site, back trajectories were calculated using the HYSPLIT model (Stein et al., 2015) for every second hour. They were calculated for a height of 50 m above the ground and started 48 hours earlier before the air arrived at the measurement site. Calculations for different heights (500 m and 1000 m) gave similar results as the trajectories calculated for a height of 50 m. To extract information about the relation between the source of air masses and the measurements, the cluster analysis tool of the HYSPLIT model was used, which classified the trajectories into two groups (Fig. 2).

Trajectories showed most often prevailing long-distance transport of air masses from the southwest, from which they traveled hundreds of kilometers from the Atlantic Ocean (approximately 1000 km away from the measurement site) within 48 hours. These air masses were likely influenced by marine and continental emissions as they crossed over northern France and Belgium. They are referred to hereafter as belonging to the long-range transport group. The other group of trajectories did not show a prevalent direction but shared the common feature that these air masses circulated over the cities nearby the measurement site, e.g. Cologne, Düsseldorf, and Frankfurt (Fig. 2). These air masses are therefore influenced by regional emission sources and are referred in the following to belong to the regional transport group.
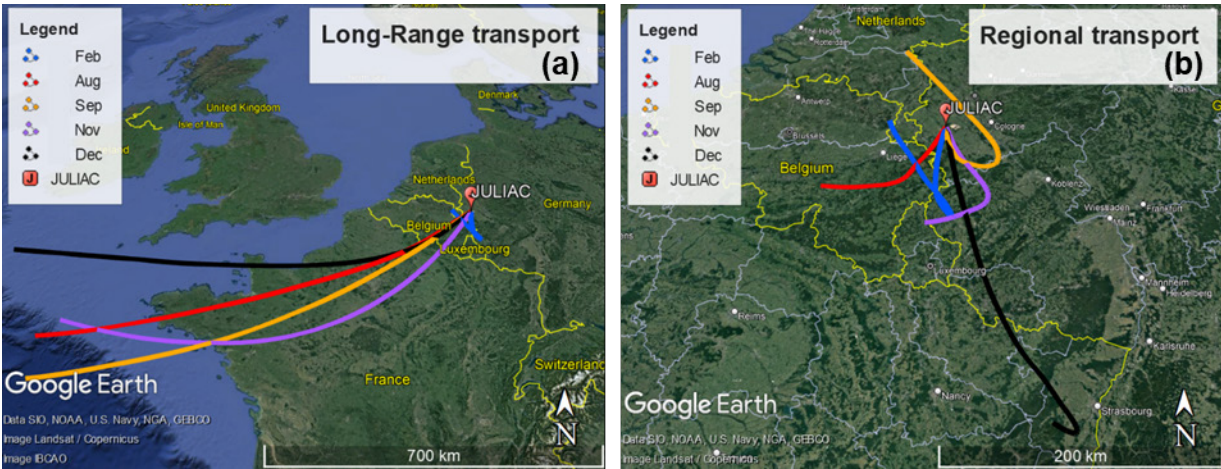
Figure 2. Results of the HYSPLIT cluster analysis of 48h back trajectories for the different measurement periods. (a) Trajectories from air masses originating from long-range transport for each period. (b) Trajectories from air masses from regional transport. © Google Maps 2022.

Fig. 3 shows mean diurnal profiles of $ClNO_2$, NO_2, O_3 concentrations, and photolysis frequencies of $ClNO_2$ in February, August, September, November, and December 2019, if measurements are split into 2 groups depending on the type of back trajectory associated to the measurement at that time. The complete

342   time series of measurements used for the analysis in this work are shown in Fig. S3-S7 (Supporting

343   Information).

344   In all cases, the diurnal profiles of $ClNO_2$ showed an increase of concentration after sunset as can be

345   expected from its chemical production during the night. Maximum concentrations were reached around

346   midnight and $ClNO_2$ concentrations remained relatively constant until sunrise, when they started to

347   decrease due to its photolysis.

348   The reaction chain to produce $ClNO_2$ at the night starts with the reaction of NO_2 and O_3. The median

349   observed O_3 showed little diurnal variation in the cold seasons (February, November, and December)

350   (Fig. 3). At this time of the year, the O_3 level was generally higher in long-range transported air (30 - 40

351   ppbv O_3) compared to regionally influenced air (15 – 20 ppbv O_3), for which ozone depletion by urban

352   NO emissions was likely more important due to fresh emissions. During summer when photochemistry

353   was most active (August, September), the median O_3 concentrations were considerably higher in

354   regionally influenced air. Ozone mixing ratios in summer showed distinct diurnal profiles with noontime

355   maxima of 80 ppbv in August and 40 ppbv in September, and nighttime values between 20 and 30 ppbv.

356   In contrast, long-range transported air exhibited a less pronounced diurnal variation in the O_3

357   concentration and mixing ratios were often only between 20 and 40 ppbv. The high summertime ozone

358   concentrations in regionally-transported air is likely due to fresh emissions of NO and VOCs, which are

359   photochemically converted to O_3.

360   The influence of fresh emissions from nearby sources is also visible in the measured NO_2 concentrations,

361   which were higher in regional air masses compared to concentrations in long-range transport air masses

362   during the entire year. For regionally-transported air masses, average nocturnal NO_2 mixing ratios were

363   around 10 ppbv in all measurement periods, except in December, when mixing ratios were lower with

364   values of about 5 ppbv. In the night, median NO_2 concentrations in long-range transported air masses

365   were generally lower than 5 ppbv in all seasons.

366   The age of the airmass could play a role in the observed levels of $ClNO_2$ due to the impact on NO_2 and O_3

367   concentrations, and hence on $ClNO_2$. As shown in Fig. 2, regionally transported air masses spend more

368   time over urban areas picking up anthropogenic emissions (indicated by high NO_2 mixing ratios). They

369   also have more time for the photochemical processing of pollutants compared to the long-range

370   transported air masses. In the cold months (February, November, and December), long reaction times

371   would lead to lower O_3 concentrations for the regional air masses due to the titration by anthropogenically

372   emitted NO compared to conditions in August and September when photochemical ozone production is

373   more efficient than the titration effect.

374 The nocturnal ClNO$_2$ concentrations were consistently lower in air masses from long-range transported

375 air compared to regional transported air in nearly all seasons except again in December. The maximum

376 median nighttime values were around 0.2 ppbv in long-range transported air and around 0.5 ppbv in air

377 masses from regional transport (Fig. 3). Only in December, no significant dependence of the ClNO$_2$

378 concentration on the origin of air masses was observed.

379 Maximum ClNO$_2$ mixing ratios of 1.6 ppbv (15-min average), which were observed at 03:00 UTC on

380 September 15 in the JULIAC campaign (Fig. S5, Supporting Information), are comparable to

381 observations in other field campaigns. In Europe, high ClNO$_2$ mixing ratios have also been observed

382 during summer in several field campaigns, in which ClNO$_2$ was measured: 0.8 ppbv near Frankfurt,

383 Germany (Phillips et al., 2012), 0.8 ppbv in London, UK (Bannan et al., 2015) and 1.1 ppbv in

384 Weybourne, UK (180 km northeast of London, (Sommariva et al., 2018)).

385
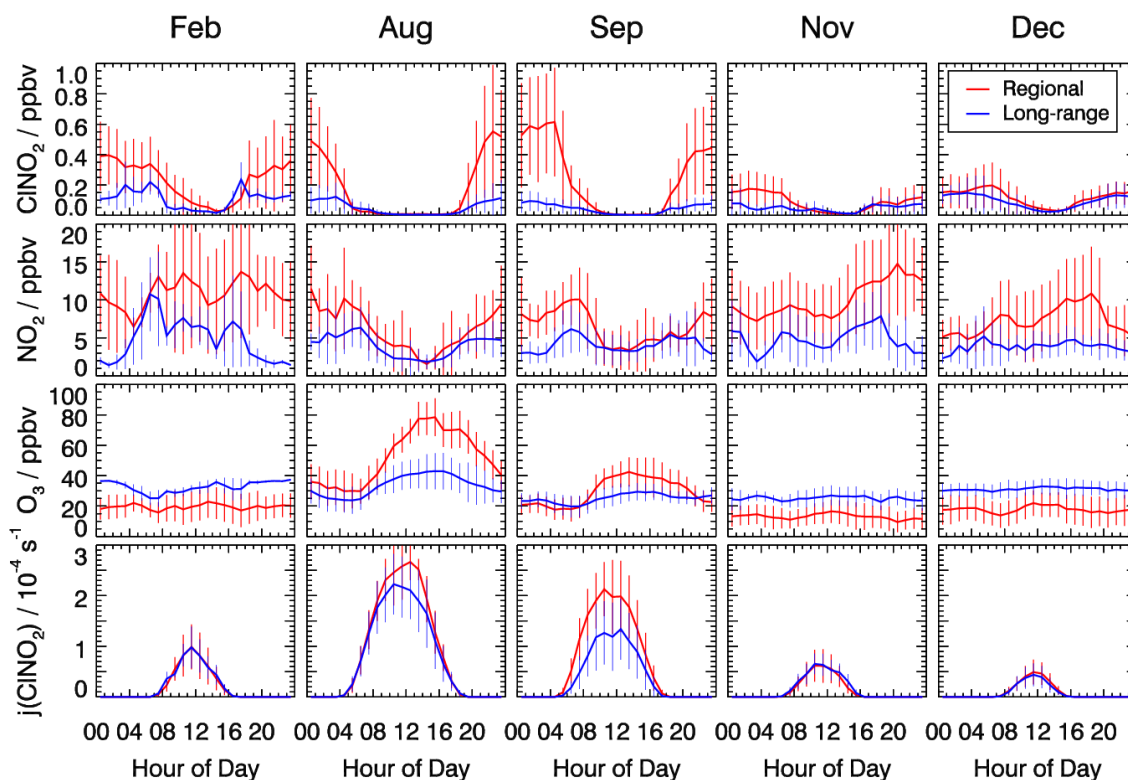
386 **Figure 3.** Mean diurnal profiles of ClNO$_2$, NO$_2$, and O$_3$ concentrations, and ClNO$_2$ photolysis

387 frequencies. Trace gas concentrations were measured in the inflowing air or values measured inside the

388 chamber were used to back-calculate concentrations in the inflowing air. Data are 1-h average values with

389 error bars denoting 1σ standard deviations.

390   The seasonally varying photolysis frequencies of $ClNO_2$ showed diurnal noontime maxima of 0.4×10^{-4} s^{-1}

391   in winter and 2.5×10^{-4} s^{-1} in summer. Sunlight lasted longest in summer and photolysis frequencies were

392   sufficiently high to destroy all $ClNO_2$ before midday. In contrast, daytime $ClNO_2$ concentrations remained

393   significantly above zero (around 30 pptv) in the cold seasons, because the maximum photolysis

394   frequencies were a least a factor of 2 lower than in summer and the duration of daylight was not long

395   enough to deplete all $ClNO_2$. Similar results were observed in wintertime measurements of $ClNO_2$ by

396   Sommariva et al. (2021).

397   Seasonal differences in $ClNO_2$ concentrations observations in this work can be compared to the seasonal

398   variations reported for measurements performed in Leicester, UK (Sommariva et al., 2018). In Leicester,

399   the highest $ClNO_2$ mixing ratio of 0.73 ppbv was observed in February, when also NO_2 mixing ratios

400   were highest with values of 43 ppbv. The seasonality of $ClNO_2$, NO_2, and O_3 observed during the

401   JULIAC campaign was different from the seasonality observed in Leicester. In this work, the highest

402    $ClNO_2$ concentrations were experienced in summer, when the air was influenced by emissions from

403   nearby cities (regional transport) resulting in high NO_2 and O_3 concentrations. The different seasonal

404   behavior in Jülich and Leicester suggests that the controlling factor for the production of $ClNO_2$ could

405   have been different in the two locations (Section 3.5).

3.3 Influence of the nocturnal vertical stratification of air on $ClNO_2$ concentrations

407   The $ClNO_2$ measurements presented in this work were obtained in air sampled at a height of 50 m above

408   ground (Section 2). While there is a well-mixed layer due to convection during the day, the cooling of the

409   ground results in weak convection of air after sunset leading to stratification of the air in the night.

410   In general, layers can be identified by the vertical profile of the potential temperature. In the night, a

411   stable surface layer (typically <20 m height) is expected to be formed, in which emissions from the

412   ground are trapped. A weakly stable nocturnal boundary layer is on top of the surface layer (NBL,

413   typically in the height range between 20 m and 200 m) and a residual layer that is fully decoupled from

414   the ground (typically height >200 m) (Brown et al., 2007). Because the tip of the inlet of the SAPHIR-

415   JULIAC inlet system was 50 m above the ground, it was most often located within the nocturnal

416   boundary layer and thus impact of surface emissions in the sampled air is expected to be small.

417   This was particularly the case in the cold seasons (Feb., Nov., and Dec.) suggesting that most of the

418   nighttime measurements presented in this work are representative of conditions in the NBL. Similar

419   conditions were encountered in the summer during nights with low wind speed and cloudless conditions.

420   However, in 8 out of 30 nights from 20 August to 20 September, the sampled air at 50 m height was

421   temporarily influenced by surface air. Indicators were, for example, observed enhancements of the NO

422   and CO concentrations, and reduced mixing ratios of $ClNO_2$.

423   An example of such an event is shown in Fig. 4 which presents measurements from the night of 21 to 22

424   August 2019. After sunset (around 19:00 UTC), a stable surface layer was formed as indicated by a

425   positive vertical temperature gradient in the lowest 20 m (Fig. 4a). Until 22:00 UTC, the surface layer

426   height increased and developed a strong temperature inversion at 30 m height. Above the surface layer,

427   the temperature gradient was slightly positive up to a height of 80 m. It is expected that for the conditions

428   until about 22:00 UTC, the measured air at 50 m height was not influenced by surface emissions. During

429   this time, $ClNO_2$ mixing ratios increased continuously to 1.5 ppbv due to chemical production. After

430   22:30 UTC, $ClNO_2$ decreased to 0.5 ppbv until 0:00 UTC. The decrease coincided with an increase in

431   wind speed from below 2 m/s at 23:00 UTC to about 4 m/s at 0:00 UTC. This might be related to the

432   phenomenon of "nocturnal jets" that can produce high wind speeds at low altitudes already in a range of

433   50 m. The elevated wind speed and change of wind direction indicate air mass came down the Rur valley

434   from Düren, a small city 10 km away from the site. At the same time, the steep temperature gradient of

435   the inversion at 30 m disappeared and most likely facilitated entrainment of surface air with lower $ClNO_2$

436   concentration. This assumption is supported by an enhanced NO mixing ratio of 0.2 ppbv observed

437   shortly before midnight, indicating ground emissions (Fig. 4(b)). At the same time, the NO_2 mixing ratio

438   increased and the O_3 mixing ratio decreased by a similar amount (10 ppbv) likely due to the chemical

439   titration of O_3 by freshly emitted NO (Fig. 4(c)). The drop of $ClNO_2$ may have been caused by the lower

440    $ClNO_2$ production in the surface layer, because N_2O_5 concentrations were low due to N_2O_5 and NO_3 loss

441   on surfaces and chemical loss in reactions with NO and organic compounds that have emission sources on

442   the ground. At later times in this night, $ClNO_2$ mixing ratios increased again to a value of 1.3 ppbv at

443   01:00 UTC (Fig. 4(b)), when the air was again sampled from within the nocturnal boundary layer, where

444   loss processes are expected to be smaller compared to the surface layer.

445
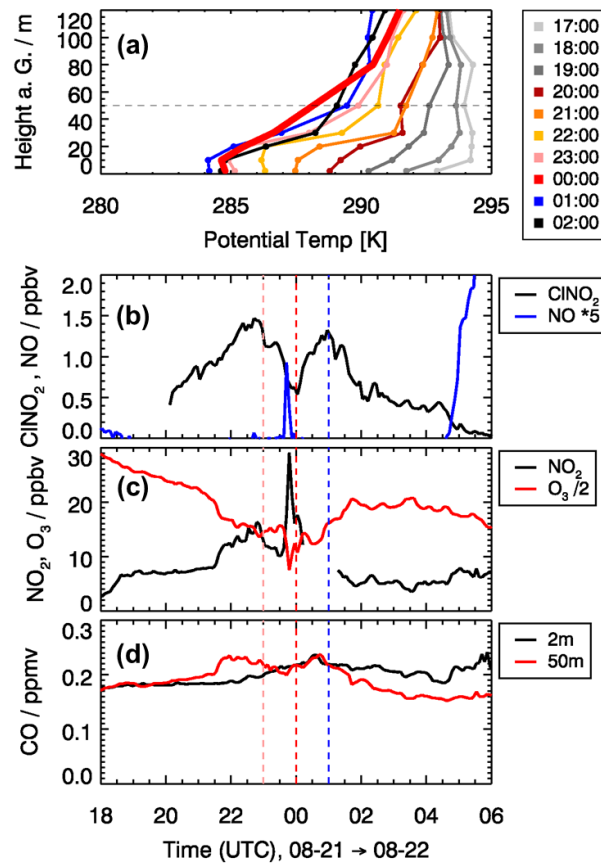
Figure 4. Impact of the vertical structure of air masses during the night from 21 to 22 August on observed
trace gas concentrations. (a): Vertical profiles of the potential temperature derived from temperature
measurements at different heights (2 m, 10 m, 20 m, 30 m, 50 m, 80 m, 100 m, 120 m). (b)-(d): $ClNO_2$,
NO, NO_2, O_3, and CO mixing ratios sampled at 50 m height with the JULIAC-SAPHIR inlet system. CO
mixing ratios were also measured at a height of 2 m. Colors of vertical lines correspond to colors of the
vertical profiles of the potential temperature.

The median diurnal profiles presented in Section 3.2 include all measurements. The ~~influence of the~~
different behavior observed ~~in~~during the night, when air was temporarily impacted by surface interaction
~~on the median values, however, is small, so that~~ only constitute a small fraction of the measurement time.
To quantify the influence of surface interactions, elevated NO concentrations at the sampling point can be
used. For more than 90% of the time, measured NO mixing ratios are lower than 0.1 ppbv (Fig. S8,
Supporting Information) indicating that air masses were typically little influenced by surface emissions.
Therefore, it can be assumed that the sampling point was most often located in the nocturnal boundary

459 layer. Mmedian values further analyzed in this work are representative of conditions in the nocturnal
460 boundary layer.

3.4 ClNO$_2$ production efficiency

462 The ClNO$_2$ production efficiency (ε) defined in Eq. 4 is affected by (1) the thermal equilibrium between
463 NO$_3$ and N$_2$O$_5$, (2) the loss of NO$_3$ + N$_2$O$_5$ by reaction of NO$_3$ with VOCs and heterogeneous uptake of
464 N$_2$O$_5$ on the aerosol surface, and (3) the yield of ClNO$_2$ from the heterogeneous reaction of N$_2$O$_5$. The
465 value of the production efficiency cannot be simply calculated because the required parameters along the
466 trajectory of the studied air mass are not known. Instead, a mean value of ε is estimated empirically from
467 the observed nocturnal increase of the ClNO$_2$ concentration at the measurement site and the
468 corresponding integrated NO$_3$ production rate. This approach assumes that there are no significant
469 nocturnal ClNO$_2$ losses in the studied air.

470 $$\varepsilon_t = \frac{([ClNO_2]_t - [ClNO_2]_{t0})}{\int_{t0}^{t} P(NO_3)_{(t)} dt} \qquad \text{(Eq. 6)}$$

471 For the calculation of the efficiency (Eq. 6) from measured ClNO$_2$ concentrations, the ClNO$_2$
472 concentration at sunset ($[ClNO_2]_{t0}$) is subtracted, because this fraction of ClNO$_2$ can be assumed to be
473 produced in the previous night. This correction is important, especially for conditions in winter and late
474 autumn, when tens of pptv of ClNO$_2$ were observed before sunset because of the long chemical lifetime
475 of ClNO$_2$ under these conditions (Fig. 3).

476 An accurate calculation of the integrated NO$_3$ production rate would require the knowledge of the NO$_2$
477 and O$_3$ concentrations while the air mass is being transported, but the exact concentrations are only
478 known at the location of the JULIAC tower. Therefore, it is necessary to make assumptions about the
479 history of the air mass. For simplification, it is here assumed that the airmass arriving at the JULIAC site
480 is homogeneous along the trajectory after sunset. This assumption requires that the consumption of NO$_2$
481 by reaction with O$_3$ is small over the integration time and that the chemical composition of the studied air
482 remains undisturbed by mixing with air masses containing different trace gas concentrations. The latter
483 assumption seems reasonable when the air is sampled above the nocturnal surface layer which was largely
484 the case during the JULIAC campaign (Section 3.3). For these assumptions, the integrated NO$_3$ radical
485 production P(NO$_3$) can be calculated from the measured NO$_2$ and O$_3$ concentrations at the measurement
486 site and the reaction rate constant (k_2) of their reaction. The value of the reaction rate constant is taken
487 from recommendations by IUPAC (Atkinson et al., 2004). Therefore, the production rate of NO$_3$ radical
488 can be substituted by the reaction rate of NO$_2$ and O$_3$ and Eq. 6 is rewritten as following:

489 $$\varepsilon_t = \frac{[ClNO_2]_t - [ClNO_2]_{t0}}{\int_{t0}^{t} k_2 [NO_2]_t [O_3]_t dt}$$ (Eq. 7)

490 t_0 can be set to the time of sunset and the time t is stepwise increased by intervals of 5 minutes (time

491 resolution of the dataset) to calculate the time series of the production efficiency in one night. For further

492 analysis, the first 4 hours after sunset is averaged for each night, because $ClNO_2$ increased to its

493 maximum concentration in most of the nights of this campaign during this time. This suggests chloride is

494 not a limiting factor for $ClNO_2$ production. Mean values of the $ClNO_2$ production efficiency in each

495 season can then be compared.

496 The $ClNO_2$ production efficiency does not show a clear seasonal behavior, but values are larger in

497 regional transported air masses than in long-range transported air masses (Fig. 5). Mean values exhibit a

498 similar pattern, if values are taken from the entire night or a period in the second half of the night (Fig.

499 8S9, Supporting Information).

500
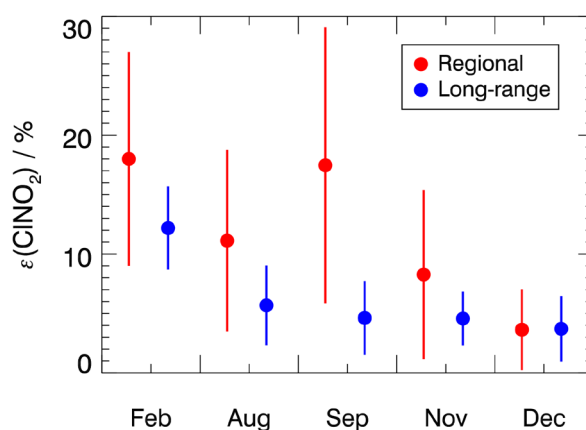
501 **Figure 5.** Mean $ClNO_2$ production efficiency for each measurement period for 4-hour average values

502 starting after sunset. Values are calculated for air masses originating either from regional or long-range

503 transportation. The vertical bars denote 1σ standard deviations.

504 For the air masses from regional transportation, the highest mean $ClNO_2$ production efficiency of

505 (18±9) % was observed in February. This is consistent with a high NO_3 production rate due to high NO_2

506 concentrations (Fig. 3), as well as the low temperatures in February which favor the formation of N_2O_5.

507 Similar $ClNO_2$ production efficiency was observed in September, although NO_2 concentrations were low.

508 This suggests that other factors, besides the ones included in Eq. 4, contributed to the efficient production

509 of $ClNO_2$ in regional air masses in September.

510   The $ClNO_2$ production efficiencies obtained in December are similar with values of (3 ± 3) % for both

511   regional and long-range transportation air masses. This is consistent with observations of $ClNO_2$, NO_2,

512   and O_3 concentrations, which were also similar regardless of the origin of air masses in December (Fig.

513   3). In the other seasons, however, the $ClNO_2$ production efficiencies were 30 to 50% lower in air masses

514   from long-range transportation compared to values obtained for regional air masses. This can be

515   explained by elevated NO_2 concentrations in regional air masses, which shifts the equilibrium between

516   NO_3 and N_2O_5 to the side of N_2O_5 and N_2O_5 and therefore facilitates the production of $ClNO_2$.

517   It should be mentioned that the production of $ClNO_2$ also requires the availability of particulate chloride

518   (Reaction R4). During the JULIAC campaign, particulate chloride concentrations were measured by an

519   aerosol mass spectrometry (AMS) instrument giving average concentrations of (0.15 ± 0.08), (0.07 ± 0.03),

520   (0.07 ± 0.06), and (0.09 ± 0.04) $\mu g/m^3$ for measurements in February, August, September and November,

521   respectively (measurements in December were not available, see Table S2 in the Supporting Information).

522   The particulate chloride measurements by the AMS instrument are restricted to non-sea-salt aerosol,

523   because the AMS was operated to measure the non-refractory particulate matters. As the measurement

524   site ~~was~~is only 200 km away from the North Sea, sea salt was likely an important source of chloride in the

525   JULIAC campaign. Thus, there was most likely more chlorine present than measured by the AMS and the

526   observed chloride concentrations must be regarded as a low limit. Nevertheless, the high $ClNO_2$

527   production efficiency in the regional air masses suggests that particulate chloride was not a limiting factor

528   for the formation of $ClNO_2$ at the measurement site (for the period of 4-hours since sunset). In the

529   following analysis, it is assumed that the availability of particulate chloride was enough to sustain

530   reaction R4 during this study, so $ClNO_2$ production was only dependent on the availability of its gas

531   phase precursors~~.~~ (see Section 3.5).

532   Previous studies have reported similar values of $ClNO_2$ production efficiencies. Two field studies

533   performed in urban environments in Canada found median values of the $ClNO_2$ production efficiency of

534   1.0 % (Mielke et al., 2016) and 0.17% (Osthoff et al., 2018). These low values were attributed to gas-

535   phase loss reactions of NO_3 competing with the formation of $ClNO_2$. In addition, the authors determined

536   significant O_3 destruction by deposition and titration in the reaction with NO in a shallow nocturnal

537   boundary layer, which further limited the production of $ClNO_2$ (Osthoff et al., 2018). In another

538   campaign, measurements were performed on board of a ship during a cruise in the Mediterranean Sea

539   (Eger et al., 2019). The $ClNO_2$ production efficiency determined from these measurements was in the

540   range between 1% and 5%, attributed to the efficient gas-phase loss of NO_3 and to the high temperature

541   (usually $>25℃$) that shifted the thermal equilibrium towards NO_3, so that little N_2O_5 was expected. In

542   contrast, the $ClNO_2$ production efficiency observed in Pasadena, U.S. (Mielke et al., 2013) was much

higher than in the field studies in Canada (median value: 9.5%). These measurements were performed in the coastal boundary layer, which was characterized by high concentrations of pollutants. The authors attributed the high $ClNO_2$ production efficiency to the rapid N_2O_5 reaction with Cl that was present in submicron aerosol particles from the redistribution of sea salt chloride as proposed by Osthoff et al. (2008).

3.5 Dependence of the $ClNO_2$ production on the availability of NO_2 and O_3

Most of the measurements taken during nighttime ~~sampling~~ from a height of 50 m were not affected by fresh local emissions from the ground surface, as discussed in Section 3.2. ~~In addition~~As first approximation, it can be assumed that particulate chloride is not limiting the formation of $ClNO_2$ (Section 3.4). Therefore, the amount of $ClNO_2$ that can be formed during the night is a function of the amounts of NO_2 and O_3 available at sunset. The dependence of the $ClNO_2$ production on the availability of NO_2 and O_3 for ambient conditions is further investigated by box model calculations. This method was previously used by Sommariva et al. (2018) and a detailed description can be found in their work. In brief, the model is initialized with a matrix of ~~multiple~~ initial NO_2 and O_3 concentrations. The chemical box model includes production and loss reactions of $ClNO_2$ (Reaction R1- R4, reactions rate constants are taken from ~~recommendations in).~~the IUPAC recommendations (Atkinson et al., 2004)). $ClNO_2$ concentrations are calculated for each initial NO_2 and O_3 concentrations after 4 hours. This length of the simulation is chosen, because observed $ClNO_2$ concentrations typically reached their maximum values approximately 4 hours after sunset in the JULIAC campaign.

~~Following , a constant NO_3 loss rate constant of 0.001 s^{-1} is used to represent the typical loss of NO_3 radicals in the reaction with organic compounds (Reaction R5).~~ In the model, the efficiency of the conversion of N_2O_5 to $ClNO_2$ is assumed to be constant, with a value for the uptake coefficient of N_2O_5 of 0.01 from Bertram and Thornton (2009), and a $ClNO_2$ yield of 0.5 (Reaction R4) from Roberts et al. (2009). The aerosol surface area (S_a) measured during JULIAC was in the order of 100 $\mu m^2/cm^3$ (~~data not shown~~Table S1) and was set to this constant value in the model. Temperature was fixed at 22 °C to represent typical summer-like conditions. Hence, the pseudo-first order reaction rate constant for N_2O_5 uptake is 6.0×10^{-5} s^{-1}. Following Sommariva et al. (2018), a constant NO_3 loss rate is used to represent the typical loss of NO_3 radicals (k_{NO3}) in their reactions with organic compounds (Reaction R5). The assumed value of the NO_3 loss rate, k_{NO3}, is adjusted, so that the modelled $ClNO_2$ concentration agrees with the magnitude of the observations (Fig. S10, Supporting Information), which corresponds to an NO_3 reactivity of 0.004 s^{-1}. It should be noted that the purpose of such simplified model is to examine the idealized dependence of $ClNO_2$ on the chemical conditions, not to reproduce the measurements.

575 Fig. 6(a) shows the modelled $ClNO_2$ mixing ratios ~~depending on~~as a function of the initial NO_2 and O_3

576 concentrations at sunset. Given the chemical conditions of long-range transported air masses in summer

577 (25 to 35 ppbv O_3 and 4 to 5 ppbv of NO_2), the model predicts $ClNO_2$ mixing ratios in the range of 0.4~~1~~ to

578 0.~~6~~16 ppbv. Because of the simplifications adopted in the modelling approach, calculated $ClNO_2$ mixing

579 ratios tend to underestimate ~~are approximately a factor of 2-3 higher than~~ the measurements, which are

580 around 0.2-0.3 ppbv (Fig. ~~3~~S10). For regional air masses containing higher NO_2 mixing ratios~~,~~ (6 to 10

581 ppbv of NO_2), NO_3 production rates and therefore also calculated $ClNO_2$ mixing ratios are higher (~~Fig.~~

582 ~~6(a)). Although the variability of the observed NO_2 and O_3 mixing ratios is high in regional air masses,~~

583 ~~calculated $ClNO_2$ mixing ratios are in a narrow range of values~~ between 0.~~6 and 1.~~2 and 0.4 ppbv~~.~~, Fig.

584 6(a)). Given the ~~location~~position of each measurement periods in the isopleth plot, it ~~appears~~can be

585 concluded that all long-range transported air masses ~~are~~tend to be NO_2 limited while the regional

586 transported air masses ~~are~~tend to be NO_2 limited in summer/autumn and O_3 limited in winter.

587 To further interpret the controlling factors of $ClNO_2$ production, the dependence of $ClNO_2$ production

588 efficiency ε on NO_2 and O_3 is presented in Fig. 6 (c). The modelled $ClNO_2$ production efficiency

589 increases with increasing mixing ratios of NO_2 but not with increasing O_3 (Fig. 6 (c)) as expected from

590 Eq. 4, which shows that the $ClNO_2$ production efficiency is a function of multiple parameters but not of

591 the O_3 mixing ratio. In general, the model reproduces the experimentally determined $ClNO_2$ production

592 efficiency (as shown in Fig. 5) within the uncertainty of the calculation (30% to 40%), which is mainly

593 due to the assumptions concerning the history of air masses (Section 3.4). However, the relatively high

594 $ClNO_2$ production efficiency found in August and September in the regional air masses (Fig. 5) is

595 significantly underestimated by the model. The discrepancy suggests that other processes facilitate the

596 conversion from NO_3 to $ClNO_2$ in the regional air masses for summer-like conditions. Though the

597 purpose of this model calculation is not to reproduce the observations, it is critical to address the related

598 uncertainties/limitations due to the assumptions in the simplified model. The key parameters affecting the

599 formation of $ClNO_2$ concentrations are temperature, NO_3 loss, N_2O_5 loss. Their impact on the model

600 results is discussed below.

601 Fig. 6(b) shows the dependence of modelled $ClNO_2$ on the temperature and NO_2 concentrations

602 investigated by the same model approach, for which the O_3 concentration is fixed to 30 ppbv

603 (representing typical O_3 level of long-range transported air). In this case, the modelled $ClNO_2$

604 concentrations reach maximum values at temperatures of 5 ℃. For these winter-like conditions, the low

605 temperature shifts the equilibrium between NO_3 to N_2O_5 to the side of N_2O_5. In contrast, the conversion of

606 NO_2 to $ClNO_2$ is suppressed at high temperatures (T > 15℃) as typical conditions in August and

607 September. Temperature also plays an important role for the value of the $ClNO_2$ production efficiency

608 due to the shift of the equilibrium between NO$_3$ to N$_2$O$_5$. The significantly higher ClNO$_2$ production

609 efficiency observed in February compared to the other seasons could be largely attributed to the low

610 temperature at that time (Fig. ~~as typical conditions in August and September.~~6(d)).

611
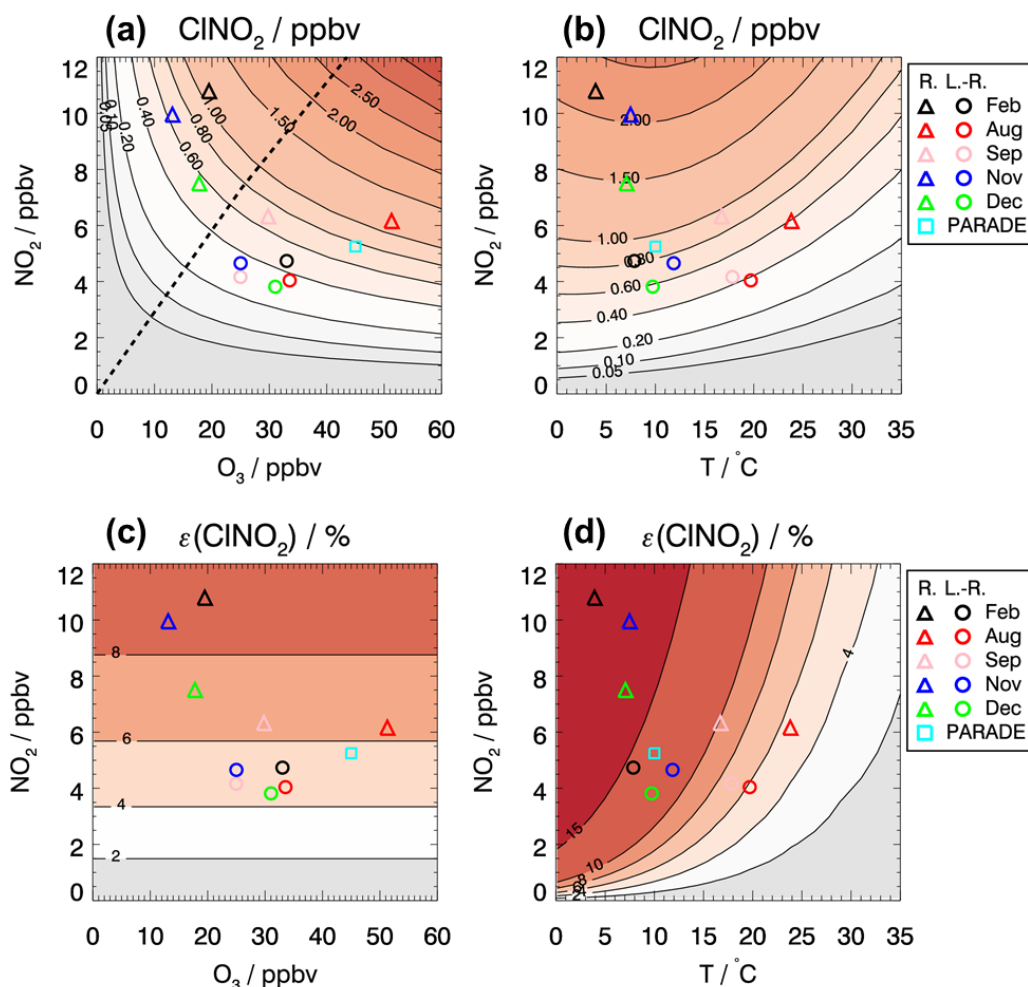
612 Sensitivity tests demonstrate that decreasing the rate of the chemical loss of NO$_3$ to organic compounds

613 (Fig. S11, Supporting Information) only have small impact, while the seasonal variation of chemical loss

614 of NO$_3$ peaks in summer-like conditions due to the intense biogenic emission. , The higher production

615 efficiency could be attributed to faster than assumed conversion from N$_2$O$_5$ to ClNO$_2$, which can bring

616 modelled and measured valued into agreement. This can be either achieved by increasing the value of the

617 N$_2$O$_5$ uptake coefficient (Fig. S12, Supporting Information) or the yield of ClNO$_2$ in the process of the

618 heterogeneous uptake of N$_2$O$_5$ on aerosol (Fig. S13, Supporting Information).

619 As mentioned above, the NO$_3$ reactivity is assumed to be 0.004 s^{-1} to match the observations, which is

620 comparable to the NO$_3$ reactivity observed at a mountainous site in south Germany with a campaign-

621   averaged value of 0.01 s^{-1} for nighttime conditions (up to 0.3 s^{-1}) (Liebmann et al., 2018). As shown in the

622   sensitivity test, a higher NO_3 reactivity leads to lower modelled $ClNO_2$ concentrations. Therefore, the low

623   NO_3 reactivity in the model could be regarded as a lower limit given the similar biogenic-influenced

624   environments.

625   In this model calculation, the aerosol surface area S_a is held constant instead of using the value measured

626   inside the chamber, which was likely impacted by the sampling system but cannot be corrected for

627   ambient measurement (Section 2.3). Nevertheless, the measured S_a gives some confidence that the model

628   is not using an unrealistic lower limit.

629   The aerosol chemical composition also plays a role in determining the production efficiency. The yield of

630    $ClNO_2$ from N_2O_5 heterogenous reaction ($\varphi(ClNO_2)$) can be expressed by assuming that the production

631   of $ClNO_2$ results from the competition between Cl^- and H_2O reacting with the $H_2ONO_2^+$ intermediate

632   formed from the N_2O_5 uptake on aerosol (Bertram and Thornton, 2009;Mielke et al., 2013;McDuffie et

633   al., 2018b).

634    $$\varphi(ClNO_2)_{par} = \left(1 + \frac{[H_2O]}{50[Cl^-]}\right)^{-1} \qquad\qquad\qquad\qquad\qquad\qquad\text{(Eq. 8)}$$

635   The value of the $ClNO_2$ yield is different in the periods of the campaign showing maximum values of 0.6

636   to 0.8 in February (Fig. S14). This is consistent with the relatively high $ClNO_2$ production efficiency

637   derived from the integrated production rate of NO_3 (Eq.7). However, the calculated $ClNO_2$ yield

638   decreases below 0.4 in August and September, which could be attributed to the higher aerosol liquid

639   water content in these two periods compared to the value in other periods (Table S1). The calculated

640    $ClNO_2$ yield is also higher for the long-range transported air masses than those for the regional one (Fig.

641   S14, Supporting Information). The relatively high $ClNO_2$ production efficiencies found in the regional air

642   masses, which are in contrast to their relatively low calculated $\varphi(ClNO_2)$, suggest that other factors play

643   an important role in determining the $ClNO_2$ production such as larger-than-assumed uptake coefficient for

644   N_2O_5 and/or aerosol surface area.
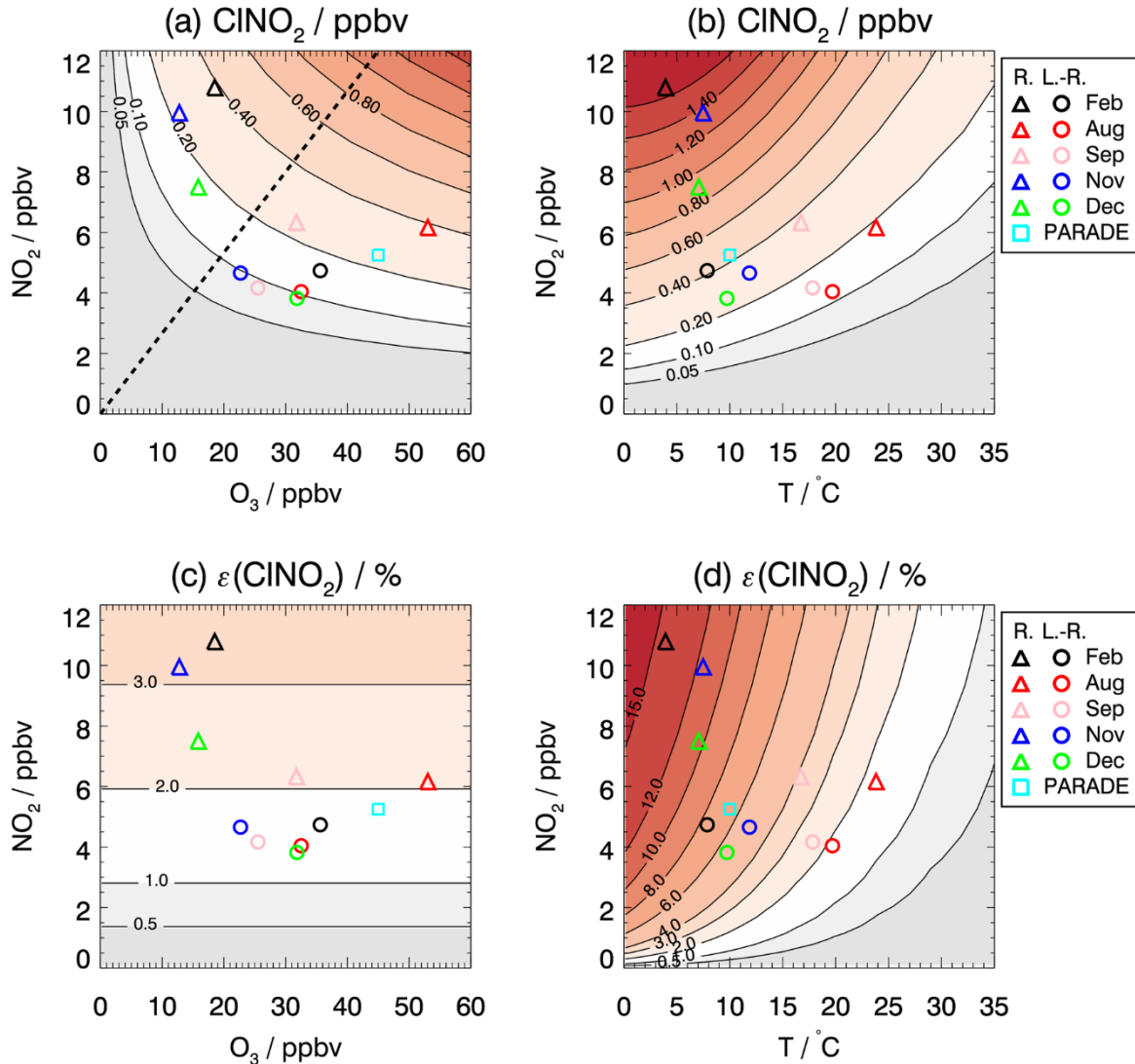
Figure 6. Isopleth plot of modelled (a, b) $ClNO_2$ mixing ratios that accumulate during nighttime and (c, d) the $ClNO_2$ production efficiency depending on (a, c) the initial O_3 and NO_2 mixing ratios and (b, d) the temperature and initial NO_2 mixing ratios. Values are taken after four hours ~~after~~since sunset, when maximum $ClNO_2$ concentrations were ~~reached in the campaign~~observed. Symbols mark calculated $ClNO_2$ mixing ratios for average values of NO_2 and O_3 mixing ratios measured in each period of the JULIAC campaign, if air masses originated either from long-range (L.-R.) or regional (R.) transportation. For comparison, values are also shown for measurements during the PARADE campaign in summer in Germany (Phillips et al., 2012). The dashed line (panel a) separates the regimes for which $ClNO_2$ production is more sensitive to the change of O_3 (upper left) and NO_2 (bottom right).

655 To further interpret the controlling factor of $ClNO_2$ production, the dependence of $ClNO_2$ production

656 efficiency ϵ on NO_2, O_3, and temperature is presented in Fig. 6 (c) and (d). The modelled $ClNO_2$

657 production efficiency increases with increasing mixing ratios of NO_2 but not with increasing O_3 (Fig. 6

658 (c)) as expected from Eq. 4, which shows that the $ClNO_2$ production efficiency is a function of multiple

659 parameters but not of the O_3 mixing ratio. Temperature also plays an important role for the value of the

660 $ClNO_2$ production efficiency due to the shift of the equilibrium between NO_3 to N_2O_5. The significantly

661 higher $ClNO_2$ production efficiency observed in February compared to the other seasons could be largely

662 attributed to the low temperature at that time (Fig. 6(d)).

663 In general, the model reproduces the experimentally determined $ClNO_2$ production efficiency (as shown

664 in Fig. 5) within the uncertainty of the calculation of 30% to 40%, which is mainly due to the assumptions

665 concerning the history of air masses (Section 3.4). However, the relatively high $ClNO_2$ production

666 efficiency found in August and September in the regional air masses (Fig. 5) is significantly

667 underestimated by the model. The large discrepancy indicates other processes facilitated the conversion

668 from NO_3 to $ClNO_2$ in the regional air masses for summer-like conditions. In fact, sensitivity tests

669 demonstrate that decreasing the rate of the chemical loss of NO_3 (Fig. S9, Supporting Information) could

670 not help, but faster than assumed conversion from N_2O_5 to $ClNO_2$ can bring modelled and measured

671 valued into agreement. This can be either achieved by increasing the value of the N_2O_5 uptake coefficient

672 (Fig. S10, Supporting Information) or the yield of $ClNO_2$ in the process of the heterogeneous uptake of

673 N_2O_5 on aerosol (Fig. S11, Supporting Information).

674 For comparison, the observation from another field campaign conducted in a similar rural environment in

675 Germany is marked in the isopleth diagram (Fig. 6). The PARADE campaign took place in the Taunus

676 Observatory of the University of Frankfurt located 170 km southeast of the JULIAC measurement site

677 (Phillips et al., 2012). The maximum observed $ClNO_2$ mixing ratios wereratio was 0.8 ppbv when the

678 measurement site was influenced by air masses from the UK/North Sea. This value is comparable tolower

679 than the results of the model calculations using the median NO_2 and O_3 observed in that campaign, which

680 is consistent to the general underprediction for summer-like conditions for the JULIAC campaign,

681 suggesting the conversion from NO_3 to $ClNO_2$ is more efficient than the model predicts in summer. The

682 position in the isopleth diagram suggests that $ClNO_2$ formation was limited by the availability of NO_2

683 similar to the summer period the JULIAC campaign, the same season as the PARADE campaign

684 (August)..).

4 Summary and Conclusions

Concentrations of $ClNO_2$ and other trace gases and the chemical composition of aerosols were measured during the Jülich Atmospheric Chemistry Project (JULIAC) campaign in 2019 performed at a rural site in Germany. Ambient air was sampled into the atmospheric simulation chamber SAPHIR from a height of 50 m, which, for most of the time, was uncoupled from surface layer during the night. Chamber characterization experiments demonstrated that no significant loss or production of $ClNO_2$ occurred inside the chamber for experimental conditions of the JULIAC campaign.

In all periods, $ClNO_2$ measurements showed a trend of increasing mixing ratios after sunset with maximum values were reached around midnight. This qualitative behavior is consistent with the chemical production of $ClNO_2$ and insignificant losses during the night. Photolysis was the main loss process for $ClNO_2$ on the following day. The maximum $ClNO_2$ concentration in this campaign of 1.6 ppbv was observed in September at the late-night (03:00 UTC). The analysis of the origin of air masses by calculations of back trajectories shows that mixing ratios of $ClNO_2$, NO_2 and O_3 were higher in regional air masses than in air masses that traveled a long distance.

A case study analyzing measurements in the night from 21 to 22 August 2019 shows that the stratification of layers during the night can strongly impact observed trace gas concentrations, specifically when the sampling point of the inlet system was located within a height range that was characterized by poor vertical mixing of the air. During most times of the campaign, however, the sampling point was isolated from the surface layer during the night. In this case, losses of trace gases to the surface and reactions with fresh emissions on the ground, which would typically reduce $ClNO_2$ production, were not important.

The $ClNO_2$ production efficiency (i.e. the number of $ClNO_2$ molecules formed per produced NO_3 molecule) was higher for conditions in air masses from regional areas than from long-range transportation, mostly due to the higher NO_2 mixing ratios. The minimum average value of the production efficiency calculated for the individual measurement periods in the JULIAC campaign was 3%, experienced in December for all air masses independent from their origin. This low value can be attributed to the low NO_2 mixing ratios experienced in winter. For the air masses from long-range transportation, the mean $ClNO_2$ production efficiencies were in the range of 3% to 6% in the period between August to November but were as high as 12% in February, consistent with the seasonality of the observed $ClNO_2$ concentrations. The highest mean $ClNO_2$ production efficiency was found in February, when values reached (18±9) % and NO_2 concentrations were highest in the regional air masses. High $ClNO_2$ production efficiency was also found in September, when NO_2 concentrations were low, suggesting that other factors including the available aerosol surface area, (S_a), the variability of the N_2O_5

717 uptake coefficient, and the yield of $ClNO_2$ in the heterogeneous reaction of N_2O_5 were favoring the

718 production of $ClNO_2$.

719 With the help of a simple box model of nighttime chemistry for the NO_3-N_2O_5-$ClNO_2$ system, the

720 dependence of $ClNO_2$ concentration on the availability of O_3 and NO_2 was investigated. The purpose of

721 such simplified model is to demonstrate the general feature of ClNO2 production versus chemical

722 conditions but not to compare with observations. The model results suggest that $ClNO_2$ production was

723 more sensitive to the availability of NO_2 than that of O_3, especially the air masses from long-range

724 transportation. The seasonal variability of $ClNO_2$ is less pronounced compared to the seasonal changes of

725 NO_2 and O_3 concentrations, because changes in the NO_2 and O_3 concentrations partly compensated for

726 each other. The simple model cannot predict the seasonal changes in the observed $ClNO_2$ mixing ratios.

727 This indicates that processes other than the NO_3 production rate significantly impacted the $ClNO_2$ mixing

728 ratios. Nevertheless, this simple model approach helps to understand the general features of the

729 dependence of $ClNO_2$ concentrations on the availability of NO_2 and O_3 in the JULIAC campaign.

730

Data availability

732 The data used in this study are available on the Jülich DATA platform (https://doi.org/10.26165/JUELICH-
733 DATA/XG6YGZ).

Author contributions

735 AH designed JULIAC campaign and organized it together with HF and FH. ZT and RS performed the

736 measurements of $ClNO_2$ and analyzed the data. ZT, RS, HF, and AH wrote the paper. All co-authors

737 contributed with data and commented and discussed the manuscript and contributed to the writing of the

738 manuscript.

Competing interests

740 Some authors are members of the editorial board of Atmospheric Chemistry and Physics. The authors

741 declare that they have no conflict of interest.

Acknowledgements

743 The authors thank the scientific team of JULIAC campaign for logistical support, the Chemistry

744 Workshop and Glassblower of the University of Leicester for technical support

745 **Financial Support.**

746 This project has been supported by the BMBF project ID-CLAR (grant no. 01DO17036) and BMBF project

747 PRACTICE (grant no. 01LP1929A), the European Research Council (ERC) and European Commission

748 (EC) under the European Union's Horizon 2020 research and innovation program (SARLEP grant

749 agreement no. 681529 and Eurochamp 2020 grant agreement no. 730997),.).

750

References:

752 Atkinson, R., Baulch, D. L., Cox, R. A., Crowley, J. N., Hampson, R. F., Hynes, R. G., Jenkin, M. E.,
753   Rossi, M. J., and Troe, J.: Evaluated kinetic and photochemical data for atmospheric chemistry:
754   Volume I - gas phase reactions of Ox, HOx, NOx and SOx species, Atmos. Chem. Phys., 4, 1461-
755   1738, 10.5194/acp-4-1461-2004, 2004.

756 Bannan, T. J., Booth, A. M., Bacak, A., Muller, J. B. A., Leather, K. E., Le Breton, M., Jones, B.,
757   Young, D., Coe, H., Allan, J., Visser, S., Slowik, J. G., Furger, M., Prévôt, A. S. H., Lee, J.,
758   Dunmore, R. E., Hopkins, J. R., Hamilton, J. F., Lewis, A. C., Whalley, L. K., Sharp, T., Stone,
759   D., Heard, D. E., Fleming, Z. L., Leigh, R., Shallcross, D. E., and Percival, C. J.: The first UK
760   measurements of nitryl chloride using a chemical ionization mass spectrometer in central London
761   in the summer of 2012, and an investigation of the role of Cl atom oxidation, J. Geophys. Res.,
762   120, 5638-5657, 10.1002/2014JD022629, 2015.

763 Bertram, T. H., and Thornton, J. A.: Toward a general parameterization of N2O5 reactivity on aqueous
764   particles: the competing effects of particle liquid water, nitrate and chloride, Atmos. Chem. Phys.,
765   9, 8351-8363, 10.5194/acp-9-8351-2009, 2009.

766 Bohn, B., Rohrer, F., Brauers, T., and Wahner, A.: Actinometric measurements of NO2 photolysis
767   frequencies in the atmosphere simulation chamber SAPHIR, Atmos. Chem. Phys., 5, 493-503,
768   10.5194/acp-5-493-2005, 2005.

769 Brown, S. S., Dubé, W. P., Osthoff, H. D., Wolfe, D. E., Angevine, W. M., and Ravishankara, A. R.:
770   High resolution vertical distributions of NO$_3$ and N$_2$O$_5$
771   through the nocturnal boundary layer, Atmos. Chem. Phys., 7, 139-149, 10.5194/acp-7-139-2007,
772   2007.

773 Brown, S. S., and Stutz, J.: Nighttime radical observations and chemistry, Chem. Soc. Rev., 41, 6405-
774   6447, 10.1039/c2cs35181a, 2012.

775 Eger, P. G., Friedrich, N., Schuladen, J., Shenolikar, J., Fischer, H., Tadic, I., Harder, H., Martinez, M.,
776   Rohloff, R., Tauer, S., Drewnick, F., Fachinger, F., Brooks, J., Darbyshire, E., Sciare, J., Pikridas,
777   M., Lelieveld, J., and Crowley, J. N.: Shipborne measurements of ClNO2 in the Mediterranean
778   Sea and around the Arabian Peninsula during summer, Atmos. Chem. Phys., 19, 12121-12140,
779   10.5194/acp-19-12121-2019, 2019.

George, I. J., and Abbatt, J. P. D.: Heterogeneous oxidation of atmospheric aerosol particles by gas-phase radicals, Nat. Chem., 2, 713, 10.1038/nchem.806, 2010.

Jeong, D., Seco, R., Gu, D., Lee, Y., Nault, B. A., Knote, C. J., McGee, T., Sullivan, J. T., Jimenez, J. L., Campuzano-Jost, P., Blake, D. R., Sanchez, D., Guenther, A. B., Tanner, D., Huey, L. G., Long, R., Anderson, B. E., Hall, S. R., Ullmann, K., Shin, H., Herndon, S. C., Lee, Y., Kim, D., Ahn, J., and Kim, S.: Integration of airborne and ground observations of nitryl chloride in the Seoul metropolitan area and the implications on regional oxidation capacity during KORUS-AQ 2016, Atmos. Chem. Phys., 19, 12779-12795, 10.5194/acp-19-12779-2019, 2019.

Kercher, J., Riedel, T., and Thornton, J.: Chlorine activation by N2O5: simultaneous, in situ detection of ClNO2 and N2O5 by chemical ionization mass spectrometry, Atmos. Meas. Tech., 2, 193-204, 10.5194/amt-2-193-2009, 2009.

Le Breton, M., Hallquist, Å. M., Pathak, R. K., Simpson, D., Wang, Y., Johansson, J., Zheng, J., Yang, Y., Shang, D., Wang, H., Liu, Q., Chan, C., Wang, T., Bannan, T. J., Priestley, M., Percival, C. J., Shallcross, D. E., Lu, K., Guo, S., Hu, M., and Hallquist, M.: Chlorine oxidation of VOCs at a semi-rural site in Beijing: significant chlorine liberation from ClNO2 and subsequent gas- and particle-phase Cl–VOC production, Atmos. Chem. Phys., 18, 13013-13030, 10.5194/acp-18-13013-2018, 2018.

Liebmann, J. M., Muller, J. B. A., Kubistin, D., Claude, A., Holla, R., Plass-Dülmer, C., Lelieveld, J., and Crowley, J. N.: Direct measurements of NO3 reactivity in and above the boundary layer of a mountaintop site: identification of reactive trace gases and comparison with OH reactivity, Atmos. Chem. Phys., 18, 12045-12059, 10.5194/acp-18-12045-2018, 2018.

Liu, X., Qu, H., Huey, L. G., Wang, Y., Sjostedt, S., Zeng, L., Lu, K., Wu, Y., Hu, M., Shao, M., Zhu, T., and Zhang, Y.: High Levels of Daytime Molecular Chlorine and Nitryl Chloride at a Rural Site on the North China Plain, Environ. Sci. Technol., 51, 9588-9595, 10.1021/acs.est.7b03039, 2017.

Lou, S., Tan, Z., Gan, G., Chen, J., Wang, H., Gao, Y., Huang, D., Huang, C., Li, X., Song, R., Wang, H., Wang, M., Wang, Q., Wu, Y., and Huang, C.: Observation based study on atmospheric oxidation capacity in Shanghai during late-autumn: Contribution from nitryl chloride, Atmos. Environ., 271, 118902, 10.1016/j.atmosenv.2021.118902, 2022.

McDuffie, E. E., Fibiger, D. L., Dubé, W. P., Lopez-Hilfiker, F., Lee, B. H., Thornton, J. A., Shah, V., Jaeglé, L., Guo, H., Weber, R. J., Michael Reeves, J., Weinheimer, A. J., Schroder, J. C., Campuzano-Jost, P., Jimenez, J. L., Dibb, J. E., Veres, P., Ebben, C., Sparks, T. L., Wooldridge, P. J., Cohen, R. C., Hornbrook, R. S., Apel, E. C., Campos, T., Hall, S. R., Ullmann, K., and Brown, S. S.: Heterogeneous N2O5 Uptake During Winter: Aircraft Measurements During the 2015 WINTER Campaign and Critical Evaluation of Current Parameterizations, J. Geophys. Res., 123, 4345-4372, 10.1002/2018jd028336, 2018a.

McDuffie, E. E., Fibiger, D. L., Dubé, W. P., Lopez Hilfiker, F., Lee, B. H., Jaeglé, L., Guo, H., Weber, R. J., Reeves, J. M., Weinheimer, A. J., Schroder, J. C., Campuzano-Jost, P., Jimenez, J. L., Dibb, J. E., Veres, P., Ebben, C., Sparks, T. L., Wooldridge, P. J., Cohen, R. C., Campos, T., Hall, S. R., Ullmann, K., Roberts, J. M., Thornton, J. A., and Brown, S. S.: ClNO2 Yields From Aircraft Measurements During the 2015 WINTER Campaign and Critical Evaluation of the Current Parameterization, J. Geophys. Res., 123, 12,994-913,015, 10.1029/2018jd029358, 2018b.

821 McNamara, S. M., Kolesar, K. R., Wang, S., Kirpes, R. M., May, N. W., Gunsch, M. J., Cook, R. D.,
822   Fuentes, J. D., Hornbrook, R. S., Apel, E. C., China, S., Laskin, A., and Pratt, K. A.: Observation
823   of Road Salt Aerosol Driving Inland Wintertime Atmospheric Chlorine Chemistry, ACS Cent.
824   Sci., 6, 684-694, 10.1021/acscentsci.9b00994, 2020.

825 Mielke, L. H., Furgeson, A., and Osthoff, H. D.: Observation of ClNO2 in a mid-continental urban
826   environment, Environ. Sci. Technol., 45, 8889-8896, 10.1021/es201955u, 2011.

827 Mielke, L. H., Stutz, J., Tsai, C., Hurlock, S. C., Roberts, J. M., Veres, P. R., Froyd, K. D., Hayes, P.
828   L., Cubison, M. J., Jimenez, J. L., Washenfelder, R. A., Young, C. J., Gilman, J. B., de Gouw, J.
829   A., Flynn, J. H., Grossberg, N., Lefer, B. L., Liu, J., Weber, R. J., and Osthoff, H. D.:
830   Heterogeneous formation of nitryl chloride and its role as a nocturnal NOx reservoir species
831   during CalNex-LA 2010, J. Geophys. Res., 118, 10,638-610,652, 10.1002/jgrd.50783, 2013.

832 Mielke, L. H., Furgeson, A., Odame-Ankrah, C. A., and Osthoff, H. D.: Ubiquity of ClNO2 in the
833   urban boundary layer of Calgary, Alberta, Canada, Can. J. Chem., 94, 414-423, 10.1139/cjc-2015-
834   0426, 2016.

835 Osthoff, H. D., Roberts, J. M., Ravishankara, A. R., Williams, E. J., Lerner, B. M., Sommariva, R.,
836   Bates, T. S., Coffman, D., Quinn, P. K., Dibb, J. E., Stark, H., Burkholder, J. B., Talukdar, R. K.,
837   Meagher, J., Fehsenfeld, F. C., and Brown, S. S.: High levels of nitryl chloride in the polluted
838   subtropical marine boundary layer, Nat. Geosci., 1, 324-328, 10.1038/ngeo177, 2008.

839 Osthoff, H. D., Odame-Ankrah, C. A., Taha, Y. M., Tokarek, T. W., Schiller, C. L., Haga, D., Jones,
840   K., and Vingarzan, R.: Low levels of nitryl chloride at ground level: nocturnal nitrogen oxides in
841   the Lower Fraser Valley of British Columbia, Atmos. Chem. Phys., 18, 6293-6315, 10.5194/acp-
842   18-6293-2018, 2018.

843 Phillips, G. J., Tang, M. J., Thieser, J., Brickwedde, B., Schuster, G., Bohn, B., Lelieveld, J., and
844   Crowley, J. N.: Significant concentrations of nitryl chloride observed in rural continental Europe
845   associated with the influence of sea salt chloride and anthropogenic emissions, Geophys. Res.
846   Lett., 39, 10.1029/2012gl051912, 2012.

847 Priestley, M., le Breton, M., Bannan, T. J., Worrall, S. D., Bacak, A., Smedley, A. R. D., Reyes-
848   Villegas, E., Mehra, A., Allan, J., Webb, A. R., Shallcross, D. E., Coe, H., and Percival, C. J.:
849   Observations of organic and inorganic chlorinated compounds and their contribution to chlorine
850   radical concentrations in an urban environment in northern Europe during the wintertime, Atmos.
851   Chem. Phys., 18, 13481-13493, 10.5194/acp-18-13481-2018, 2018.

852 Riedel, T. P., Wagner, N. L., Dube, W. P., Middlebrook, A. M., Young, C. J., Ozturk, F., Bahreini, R.,
853   VandenBoer, T. C., Wolfe, D. E., Williams, E. J., Roberts, J. M., Brown, S. S., and Thornton, J.
854   A.: Chlorine activation within urban or power plant plumes: Vertically resolved ClNO2 and Cl-2
855   measurements from a tall tower in a polluted continental setting, J. Geophys. Res., 118, 8702-
856   8715, 10.1002/jgrd.50637, 2013.

857 Roberts, J. M., Osthoff, H. D., Brown, S. S., Ravishankara, A. R., Coffman, D., Quinn, P., and Bates,
858   T.: Laboratory studies of products of N2O5 uptake on Cl− containing substrates, Geophys. Res.
859   Lett., 36, 10.1029/2009gl040448, 2009.

860 Rohrer, F., Bohn, B., Brauers, T., Brüning, D., Johnen, F. J., Wahner, A., and Kleffmann, J.:
861   Characterisation of the photolytic HONO-source in the atmosphere simulation chamber SAPHIR,
862   Atmos. Chem. Phys., 5, 2189-2201, 10.5194/acp-5-2189-2005, 2005.

863 Simpson, W. R., Brown, S. S., Saiz-Lopez, A., Thornton, J. A., and von Glasow, R.: Tropospheric
864   Halogen Chemistry: Sources, Cycling, and Impacts, Chem. Rev., 115, 4035-4062,
865   10.1021/cr5006638, 2015.

866 Sommariva, R., Hollis, L. D. J., Sherwen, T., Baker, A. R., Ball, S. M., Bandy, B. J., Bell, T. G.,
867   Chowdhury, M. N., Cordell, R. L., Evans, M. J., Lee, J. D., Reed, C., Reeves, C. E., Roberts, J.
868   M., Yang, M., and Monks, P. S.: Seasonal and geographical variability of nitryl chloride and its
869   precursors in Northern Europe, Atmos. Sci. Lett., 19, e844, 10.1002/asl.844, 2018.

870 Sommariva, R., Crilley, L. R., Ball, S. M., Cordell, R. L., Hollis, L. D. J., Bloss, W. J., and Monks, P.
871   S.: Enhanced wintertime oxidation of VOCs via sustained radical sources in the urban atmosphere,
872   Environ. Pollut., 274, 116563, 10.1016/j.envpol.2021.116563, 2021.

873 Stein, A. F., Draxler, R. R., Rolph, G. D., Stunder, B. J. B., Cohen, M. D., and Ngan, F.: NOAA's
874   HYSPLIT Atmospheric Transport and Dispersion Modeling System, Bull. Am. Meteorol. Soc.,
875   96, 2059-2077, 10.1175/bams-d-14-00110.1, 2015.

876 Tham, Y. J., Wang, Z., Li, Q., Yun, H., Wang, W., Wang, X., Xue, L., Lu, K., Ma, N., Bohn, B., Li,
877   X., Kecorius, S., Größ, J., Shao, M., Wiedensohler, A., Zhang, Y., and Wang, T.: Significant
878   concentrations of nitryl chloride sustained in the morning: investigations of the causes and impacts
879   on ozone production in a polluted region of northern China, Atmos. Chem. Phys., 16, 14959-
880   14977, 10.5194/acp-16-14959-2016, 2016.

881 Thornton, J. A., Kercher, J. P., Riedel, T. P., Wagner, N. L., Cozic, J., Holloway, J. S., Dube, W. P.,
882   Wolfe, G. M., Quinn, P. K., Middlebrook, A. M., Alexander, B., and Brown, S. S.: A large atomic
883   chlorine source inferred from mid-continental reactive nitrogen chemistry, Nature, 464, 271-274,
884   10.1038/nature08905, 2010.

885 Wagner, N. L., Dubé, W. P., Washenfelder, R. A., Young, C. J., Pollack, I. B., Ryerson, T. B., and
886   Brown, S. S.: Diode laser-based cavity ring-down instrument for NO_3,
887   N_2O_5, NO, NO_2 and O_3 from aircraft,
888   Atmos. Meas. Tech., 4, 1227-1240, 10.5194/amt-4-1227-2011, 2011.

889 Wagner, N. L., Riedel, T. P., Roberts, J. M., Thornton, J. A., Angevine, W. M., Williams, E. J., Lerner,
890   B. M., Vlasenko, A., Li, S. M., Dube, W. P., Coffman, D. J., Bon, D. M., de Gouw, J. A., Kuster,
891   W. C., Gilman, J. B., and Brown, S. S.: The sea breeze/land breeze circulation in Los Angeles and
892   its influence on nitryl chloride production in this region, J. Geophys. Res., 117,
893   10.1029/2012jd017810, 2012.

894 Wang, T., Tham, Y. J., Xue, L., Li, Q., Zha, Q., Wang, Z., Poon, S. C. N., Dubé, W. P., Blake, D. R.,
895   Louie, P. K. K., Luk, C. W. Y., Tsui, W., and Brown, S. S.: Observations of nitryl chloride and
896   modeling its source and effect on ozone in the planetary boundary layer of southern China, J.
897   Geophys. Res., 121, 2476-2489, 10.1002/2015JD024556, 2016.

898 Wang, X., Wang, H., Xue, L., Wang, T., Wang, L., Gu, R., Wang, W., Tham, Y. J., Wang, Z., Yang,
899   L., Chen, J., and Wang, W.: Observations of N2O5 and ClNO2 at a polluted urban surface site in

900   North China: High N2O5 uptake coefficients and low ClNO2 product yields, Atmos. Environ.,
901   156, 125-134, 10.1016/j.atmosenv.2017.02.035, 2017a.

902 Wang, Z., Wang, W., Tham, Y. J., Li, Q., Wang, H., Wen, L., Wang, X., and Wang, T.: Fast
903   heterogeneous N2O5 uptake and ClNO2 production in power plant and industrial plumes
904   observed in the nocturnal residual layer over the North China Plain, Atmos. Chem. Phys., 17,
905   12361-12378, 10.5194/acp-17-12361-2017, 2017b.

906 Yan, C., Tham, Y. J., Zha, Q., Wang, X., Xue, L., Dai, J., Wang, Z., and Wang, T.: Fast heterogeneous
907   loss of N2O5 leads to significant nighttime NOx removal and nitrate aerosol formation at a coastal
908   background environment of southern China, Sci. Total Environ., 677, 637-647,
909   10.1016/j.scitotenv.2019.04.389, 2019.

910 Young, C. J., Washenfelder, R. A., Roberts, J. M., Mielke, L. H., Osthoff, H. D., Tsai, C., Pikelnaya,
911   O., Stutz, J., Veres, P. R., Cochran, A. K., VandenBoer, T. C., Flynn, J., Grossberg, N., Haman, C.
912   L., Lefer, B., Stark, H., Graus, M., de Gouw, J., Gilman, J. B., Kuster, W. C., and Brown, S. S.:
913   Vertically resolved measurements of nighttime radical reservoirs in Los Angeles and their
914   contribution to the urban radical budget, Environ. Sci. Technol., 46, 10965-10973,
915   10.1021/es302206a, 2012.

916 Yun, H., Wang, T., Wang, W., Tham, Y. J., Li, Q., Wang, Z., and Poon, S. C. N.: Nighttime NOx loss
917   and ClNO2 formation in the residual layer of a polluted region: Insights from field measurements
918   and an iterative box model, Sci. Total Environ., 622-623, 727-734,
919   10.1016/j.scitotenv.2017.11.352, 2018.

920 Zhou, W., Zhao, J., Ouyang, B., Mehra, A., Xu, W., Wang, Y., Bannan, T. J., Worrall, S. D., Priestley,
921   M., Bacak, A., Chen, Q., Xie, C., Wang, Q., Wang, J., Du, W., Zhang, Y., Ge, X., Ye, P., Lee, J.
922   D., Fu, P., Wang, Z., Worsnop, D., Jones, R., Percival, C. J., Coe, H., and Sun, Y.: Production of
923   N2O5 and ClNO2 in summer in urban Beijing, China, Atmos. Chem. Phys., 18, 11581-11597,
924   10.5194/acp-18-11581-2018, 2018.

925